NASA / TM—2000-210594 AIAA–2001–0986

Computation of an Underexpanded 3-D Rectangular Jet by the CE / SE Method

Ching Y. Loh, Ananda Himansu, and Xiao Y. Wang
Taitech Inc., Cleveland, Ohio

Philip C.E. Jorgenson
Glenn Research Center, Cleveland, Ohio

December 2000

The NASA STI Program Office . . . in Profile

Since its founding, NASA has been dedicated to the advancement of aeronautics and space science. The NASA Scientific and Technical Information (STI) Program Office plays a key part in helping NASA maintain this important role.

The NASA STI Program Office is operated by Langley Research Center, the Lead Center for NASA's scientific and technical information. The NASA STI Program Office provides access to the NASA STI Database, the largest collection of aeronautical and space science STI in the world. The Program Office is also NASA's institutional mechanism for disseminating the results of its research and development activities. These results are published by NASA in the NASA STI Report Series, which includes the following report types:

- TECHNICAL PUBLICATION. Reports of completed research or a major significant phase of research that present the results of NASA programs and include extensive data or theoretical analysis. Includes compilations of significant scientific and technical data and information deemed to be of continuing reference value. NASA's counterpart of peer-reviewed formal professional papers but has less stringent limitations on manuscript length and extent of graphic presentations.

- TECHNICAL MEMORANDUM. Scientific and technical findings that are preliminary or of specialized interest, e.g., quick release reports, working papers, and bibliographies that contain minimal annotation. Does not contain extensive analysis.

- CONTRACTOR REPORT. Scientific and technical findings by NASA-sponsored contractors and grantees.

- CONFERENCE PUBLICATION. Collected papers from scientific and technical conferences, symposia, seminars, or other meetings sponsored or cosponsored by NASA.

- SPECIAL PUBLICATION. Scientific, technical, or historical information from NASA programs, projects, and missions, often concerned with subjects having substantial public interest.

- TECHNICAL TRANSLATION. English-language translations of foreign scientific and technical material pertinent to NASA's mission.

Specialized services that complement the STI Program Office's diverse offerings include creating custom thesauri, building customized data bases, organizing and publishing research results . . . even providing videos.

For more information about the NASA STI Program Office, see the following:

- Access the NASA STI Program Home Page at ***http://www.sti.nasa.gov***

- E-mail your question via the Internet to help@sti.nasa.gov

- Fax your question to the NASA Access Help Desk at 301–621–0134

- Telephone the NASA Access Help Desk at 301–621–0390

- Write to:
  NASA Access Help Desk
  NASA Center for AeroSpace Information
  7121 Standard Drive
  Hanover, MD 21076

NASA/TM—2000-210594 AIAA–2001–0986

Computation of an Underexpanded 3-D Rectangular Jet by the CE/SE Method

Ching Y. Loh, Ananda Himansu, and Xiao Y. Wang
Taitech Inc., Cleveland, Ohio

Philip C.E. Jorgenson
Glenn Research Center, Cleveland, Ohio

Prepared for the
39th Aerospace Sciences Meeting and Exhibit
sponsored by the American Institute of Aeronautics and Astronautics
Reno, Nevada, January 8–11, 2001

National Aeronautics and
Space Administration

Glenn Research Center

December 2000

Acknowledgments

The authors wish to thank Dr. L.S. Hultgren for fruitful discussions. This work received support from the Supersonic Propulsion Technology Project Office of NASA Glenn Research Center.

Available from

NASA Center for Aerospace Information
7121 Standard Drive
Hanover, MD 21076
Price Code: A03

National Technical Information Service
5285 Port Royal Road
Springfield, VA 22100
Price Code: A03

Available electronically at http://gltrs.grc.nasa.gov/GLTRS

AIAA-2001-0986

COMPUTATION OF AN UNDEREXPANDED 3-D RECTANGULAR JET BY THE CE/SE METHOD

Ching. Y. Loh,* **Ananda Himansu**,* **Xiao Y. Wang**,*
Taitech, Inc.
Beaver Creek, Ohio 44135

Philip C. E. Jorgenson
National Aeronautics and Space Administration, Glenn Research Center
Cleveland, Ohio 44135

Abstract

Recently, an unstructured three-dimensional space-time conservation element and solution element (CE/SE) Euler solver [1] was developed. Now it is also developed for parallel computation [2] using METIS [3] for domain decomposition and MPI (message passing interface)[4]. The method is employed here to numerically study the near-field of a typical 3-D rectangular under-expanded jet. For the computed case—a jet with Mach number $M_j = 1.6$, with a very modest grid of 1.7 million tetrahedrons, the flow features such as the shock-cell structures and the axis switching, are in good qualitative agreement with experimental results [8], [20].

1 Introduction

An under-expanded supersonic jet radiates mixing noise, broadband shock-associated noise, as well as screech tones under certain conditions. These complicated and technologically important physical phenomena have been the topic of many experimental and theoretical investigations, see Tam's review papers [10, 11] for a comprehensive list of references. Generally, the mixing noise is directly associated with large-scale structures, or instability waves, in the jet shear layer, whereas the broadband shock-associated noise and screech tones are associated with the interaction of these waves with the shock-cell structure in the jet core. The distinct screech tones arise due to a feedback loop, *i.e.*, part of the acoustic waves generated by the wave/shock-cell interaction propagate upstream and re-generate the instability waves at, or in the vicinity of, the nozzle lip. More details can be found in the review papers [9-11] and the references therein.

Jet noise is a challenging topic in computational aeroacoustics, in particular, near-field noise computation in the presence of shock cells in the jet core. In this situation, the computational scheme is required on one hand to resolve the acoustic waves without introducing too much dispersion error and numerical dissipation, while on the other hand, it is required to capture shocks, or other nonlinear phenomena, near or inside the jet correctly. In addition, non-reflecting boundary conditions must be implemented, which is more difficult to accomplish in the near field than in the far field.

The 'Space-Time Conservation Element and Solution Element Method' [5-7], or the CE/SE method for short, is a scheme that meets the above requirements. The CE/SE scheme possesses attractive properties for aeroacoustics computations in that: (*i*) it possesses low dispersion and dissipation errors; (*ii*) its 'built-in' shock-capturing nature makes the computation of shock-cell structures simple and accurate; (*iii*) the non-reflecting boundary conditions are simple and effective and can be applied in the near field of the jet without introducing excessive errors; and (*iv*) the scheme accurately predicts the vorticity, which plays an important role in the noise generating mechanism. A detailed description of the CE/SE method can be found in the reports of Chang *et al.* [6,7]. As demonstrated in our previous papers, the CE/SE scheme is well suited for computing waves on compressible shear flows [12] as well as vorticity/shock interactions [12, 13], both being corner stones of the jet-noise phenomena. Recently, the CE/SE Euler solver has been developed and used for 3-D compressible flow and aeroacoustics computations [1]. The solver is based on unstructured grids, and is robust for problems of general geometry. In order to increase the computational efficiency and to reduce the turn-around time, the 3-D Euler code has been parallelized [2] using METIS [3] for domain decomposition and MPI [4] for message passing between processors.

In this paper, the near-field of an under-expanded 3-D rectangular supersonic jet is investigated numerically

*Member AIAA

by using a CE/SE Euler solver. The paper is arranged as follows: The unstructured CE/SE Euler scheme, and the parallel computation are briefly described in Section 2. Section 3 illustrates the initial and boundary conditions for the 3-D rectangular jet problem, in particular, the novel non-reflecting boundary conditions, which are based on *flux balance*. The numerical results are presented and compared to experimental findings [8] in Section 4. Conclusions are given in Section 5.

2 The 3-D CE/SE Euler Scheme

The 3-D CE/SE method systematically solves a set of *integral* equations derived directly from the physical conservation laws, with space and time treated 'on the same footing'. Because of its integral formulation, the scheme naturally captures shocks and other discontinuities in the flow. Both dependent variables and their derivatives are solved for simultaneously and, consequently, the flow vorticity can be obtained without reduction in accuracy. Non-reflective boundary conditions are also easily implemented because of the flux-conservation formulation. Details on the 3-D CE/SE Euler method can be found in Wang *et al.*[1]. In the following subsections, the CE/SE method is briefly reviewed.

2.1 Conservation Form of the 3-D Unsteady Euler Equations

Consider a dimensionless conservation form of the unsteady 3-D Euler equations for a perfect gas. Let ρ, u, v,w, p, and γ be the density, velocity components in x, y and z directions, static pressure, and constant specific heat ratio, respectively. The Euler equations then can be written in the following vector form:

$$\boldsymbol{U}_t + \boldsymbol{F}_x + \boldsymbol{G}_y + \mathbf{H}_\mathbf{z} = \mathbf{0}, \tag{1}$$

where x, y, z and t are the spatial coordinates and time, respectively, and the conservative flow variable vector $\boldsymbol{U}$ and the flux vectors, $\boldsymbol{F}$, $\mathbf{G}$ and $\boldsymbol{H}$, are given by:

$$\boldsymbol{U} = \begin{pmatrix} U_1 \\ U_2 \\ U_3 \\ U_4 \\ U_5 \end{pmatrix}, \boldsymbol{F} = \begin{pmatrix} F_1 \\ F_2 \\ F_3 \\ F_4 \\ F_5 \end{pmatrix}, \boldsymbol{G} = \begin{pmatrix} G_1 \\ G_2 \\ G_3 \\ G_4 \\ G_5 \end{pmatrix}, \boldsymbol{H} = \begin{pmatrix} H_1 \\ H_2 \\ H_3 \\ H_4 \\ H_5 \end{pmatrix},$$

with

$$U_1 = \rho, \quad U_2 = \rho u, \quad U_3 = \rho v, U_4 = \rho w,$$

$$U_5 = p/(\gamma - 1) + \rho(u^2 + v^2 + w^2)/2$$

$$F_1 = U_2,$$

$$F_2 = (\gamma-1)U_5 + \left[(3-\gamma)U_2^2 - (\gamma-1)(U_3^2 + U_4^2)\right]/2U_1,$$

$$F_3 = U_2U_3/U_1,$$

$$F_4 = U_2U_4/U_1,$$

$$F_5 = \gamma U_2U_5/U_1 - (\gamma-1)U_2\left[U_2^2 + U_3^2 + U_4^2\right]/2U_1^2,$$

$$G_1 = U_3, \quad G_2 = U_2U_3/U_1,$$

$$G_3 = (\gamma-1)U_5 + \left[(3-\gamma)U_3^2 - (\gamma-1)(U_2^2 + U_4^2)\right]/2U_1,$$

$$G_4 = U_3U_4/U_1,$$

$$G_5 = \gamma U_3U_5/U_1 - (\gamma-1)U_3\left[U_2^2 + U_3^2 + U_4^2\right]/2U_1^2,$$

$$H_1 = U_4, \quad H_2 = U_2U_4/U_1,$$

$$H_3 = U_3U_4/U_1,$$

$$H_4 = (\gamma-1)U_5 + \left[(3-\gamma)U_4^2 - (\gamma-1)(U_2^2 + U_3^2)\right]/2U_1,$$

$$H_5 = \gamma U_4U_5/U_1 - (\gamma-1)U_4\left[U_2^2 + U_3^2 + U_4^2\right]/2U_1^2.$$

By considering (x, y, z, t) as coordinates of a four-dimensional Euclidean space, E_4, and using Gauss' divergence theorem, it follows that Eq. (1) is equivalent to the following integral conservation law:

$$\oint_{S(V)} \boldsymbol{Q}_m \cdot \mathrm{d}\mathbf{S} = \mathbf{0}, \qquad m = 1, 2, 3, 4, 5, \tag{2}$$

where $S(V)$ denotes the surface around a volume V in E_4 and $\boldsymbol{Q}_m = (F_m, G_m, H_m, U_m)$.

2.2 CE/SE Structure

In the 3-D CE/SE scheme, as in its 1-D and 2-D counterparts, the flux conservation relation in space-time is the *only* mechanism that transfers information between nodes. The conservation element, CE, is the 4-D space-time finite volume to which the integral flux condition (2) is to be applied. Solution discontinuities are allowed to occur in the interior of a conservation element. A solution element, SE, associated with a grid node is here a set of seven interface hyperplanes in E_4 that passes through this node. Note that these hyperplanes are actually 3-D space volumes or space-time volumes. The solution, *i.e.* $\boldsymbol{U}$, $\boldsymbol{U}_x$, $\boldsymbol{U}_y$, and $\mathbf{U}_\mathbf{z}$ is calculated at this node. Within a given solution element $SE(j, n)$, where j is the node index of the unstructured grid and n the number of the time step, the flow variables are not only considered continuous but are also approximated by linear Taylor expansions:

$$\boldsymbol{U}^*(x, y, z, t; j, n) = \boldsymbol{U}_j^n + (\boldsymbol{U}_x)_j^n(x - x_j) +$$

$$(\boldsymbol{U}_y)_j^n(y - y_j) + (\boldsymbol{U}_z)_j^n(z - z_j) + (\boldsymbol{U}_t)_j^n(t - t^n), \tag{3}$$

$$\boldsymbol{F}^*(x, y, z, t; j, n) = \boldsymbol{F}_j^n + (\boldsymbol{F}_x)_j^n(x - x_j) +$$

$$(\boldsymbol{F}_y)_j^n(y - y_j) + (\boldsymbol{F}_z)_j^n(z - z_j) + (\boldsymbol{F}_t)_j^n(t - t^n), \tag{4}$$

$$\boldsymbol{G}^*(x, y, z, t; j, n) = \boldsymbol{G}_j^n + (\boldsymbol{G}_x)_j^n(x - x_j) +$$

$$(\boldsymbol{G}_y)_j^n(y - y_j) + (\boldsymbol{G}_z)_j^n(z - z_j) + (\boldsymbol{G}_t)_j^n(t - t^n), \tag{5}$$

$$\boldsymbol{H}^*(x, y, z, t; j, n) = \boldsymbol{H}_j^n + (\boldsymbol{H}_x)_j^n(x - x_j) +$$

$$(\boldsymbol{H}_y)_j^n(y - y_j) + (\boldsymbol{H}_z)_j^n(z - z_j) + (\boldsymbol{H}_t)_j^n(t - t^n), \tag{6}$$

where the partial derivatives of $\boldsymbol{F}$, $\boldsymbol{G}$ and $\boldsymbol{H}$ can be related to the corresponding ones of $\boldsymbol{U}$ by using the chain rule and $\boldsymbol{U}_t$ can be directly obtained from (1).

The discrete approximation of (2) is then

$$\oint_{S(CE)} \boldsymbol{Q}_m^* \cdot \mathrm{d}\mathbf{S} = \mathbf{0}, \tag{7}$$

Each $S(CE)$ is made up by "surface segments" belonging to *two* neighboring SE's. All the unknowns are solved for based on these relations. No extrapolations (interpolations) across a stencil of cells are needed or allowed.

The CE/SE scheme is naturally adapted to the topology of an unstructured grid. In the current 3-D case, as shown in Figure 1, the four vertices A, B, C, D of any tetrahedron in an unstructured mesh form a dodecahedron along with the cell centers $N1, N2, N3$ and $N4$ of its four neighboring tetrahedrons. The cell center of the current tetrahedron $ABCD$ is O. The dodecahedron, being the projection of an E_4 space-time volume V in (2) onto the 3-D space, is formed by four hexahedrons: $O-ABD-N1$, $O-BCD-N2$, $O-CDA-N3$ and $O-ABC-N4$. These hexahedrons are the projections of space-time E_4 CE's onto 3-D space. There are totally 20 scalar unknowns $\mathbf{U}$, $\mathbf{U_x}$, $\mathbf{U_y}$, and $\mathbf{U_z}$ at O. Each of the 4 neighboring cells provides 5 scalar equations (2), totaling to 20 equations. At each marching time step, the conservative flow variables at any tetrahedron center is updated based on the flow variables at its four neighboring tetrahedron cell centers of the previous time step. Details of the procedure can be found in Wang and Chang [1].

2.3 Running the CE/SE Euler Code on a Parallel Computer

In aeroacoustic computations, due to the stringent requirement of acoustic wave resolution, a certain number of grid points (or cells) per wavelength must be maintained. Generally, with the capability of the current computers, 2-D aeroacoustics problems can be properly handled by a single processor (CPU) without excessively long run times or memory problems. However, for 3-D aeroacoustics computations, from the viewpoint of computation turn-around time and memory sizes, parallel computation with multi-processors becomes necessary.

Four steps are taken in the parallelization of the 3-D CE/SE Euler solver:

1. an unstructured grid is generated for the entire domain;

2. the domain is decomposed into subdomains according to the assigned number of processors (CPU's), using the METIS code. METIS is a mesh partitioning code in the public domain and available from the University of Minnesota [3]. It can also be freely downloaded from the web.

3. the flow is computed in each subdomain with the corresponding CPU using the CE/SE Euler solver. The CE/SE code is modified using the MPI library calls. CPU assigned to one subdomain may communicate with other CPU's assigned to the neighboring subdomains and exchange their computed results. MPI (message passing interface) is an interprocessor communication protocol standard. Public domain implementations of MPI as a software library package are prepared by the Argonne National Laboratory.

4. at the end of computation, the subdomain data is recombined.

Figure 5 is an illustrative description of the above steps. Detailed implementation of the parallelization of the CE/SE method can be found in Himansu *et al.*[2].

3 The 3-D Rectangular Jet Problem

Consider a rectangular jet as sketched in Figure 2. The aspect ratio of the nozzle is 5. The nozzle lip is allowed to have a finite thickness (3 cells) to complete the feedback loop for the possible self-sustaining screech tone. The jet Mach number, M_j, is 1.6, representing an underexpanded off-design status. The ambient flow around the jet is stationary. These conditions correspond to the experimental setup of Raman [8].

In this investigation, our attention is focussed on the near field of the jet nozzle since this is the source region for aeroacoustic noise. The inner short side width, D, of the jet nozzle is chosen as the length scale. The computational domain is a rectangular hexahedron with length, L, of $16D$, width, W, $14D$, and height, H, $5.6D$ as shown in Figure 2. The nozzle is located in the central area of the computational domain and protrudes into the domain with l =2D (Figure 2). The thickness of nozzle lip wall is 2 cells in order that a screech feedback loop can be formed. The unstructured tetrahedron grid currently used is generated by cutting a hexahedron cell into six tetrahedrons as shown in Figure 3. Currently, including the nozzle interior, there are $80 \times 60 \times 60$ such hexahrdron cells in the computational domain, which form about 1.7 million tetrahedrons. These hexahedron cells are non-uniform in size in order to have better resolution around the jet shear layers. The computational scheme is of the α-ϵ type [6,7] with $\alpha = 0$ and $\epsilon = 0.5$.

3.1 Initial Conditions

As shown in Figure 2, the convergent nozzle protrudes into the computational domain so there is some room to capture any waves that propagate upstream from the nozzle exit. A conceivable initial condition is to assume that

the pressure is uniform in the entire computational domain and equal to the ambient pressure, except at the jet nozzle exit where a higher pressure p_e is imposed as the boundary condition since the jet is under-expanded. We will also make the reasonable assumption that the temperature in the plenum equals the ambient one for this cold jet.

Let the density, axial velocity, and temperature in the jet core, be used to scale density, velocity and temperature respectively. Hence, the initial conditions in the jet core are given by

$$\rho_j = 1, \quad T_j = 1, \quad u_j = 1, \quad v_j = 0, \quad p_j = \frac{1}{\gamma M_j^2},$$

where T denotes the temperature. The initial conditions in the ambient region are given by

$$\rho_a = 1/T_a, \quad T_a = 1 + \tfrac{1}{2}(\gamma - 1)M_j^2,$$

$$u_a = 0, \quad v_a = 0, \quad p_a = \frac{1}{\gamma M_j^2},$$

where the result for the temperature follows from the assumptions of constant total enthalpy in the jet flow, and the plenum and ambient temperatures are equal.

By using the assumption of constant total enthalpy and the condition for isentropic flow, it follows that the pressure p_e at the nozzle exit can be related to the pressure p_j in the jet core by

$$\frac{p_e}{p_j} = \left[\frac{1 + \frac{1}{2}(\gamma - 1)M_j^2}{1 + \frac{1}{2}(\gamma - 1)M_e^2}\right]^{\frac{\gamma}{\gamma - 1}}.$$

Here, $M_e = 1$ is the Mach number at nozzle exit when the flow is choked.

3.2 The jet shear Layer

In the present numerical computations, no jet shear layer exists initially in the field. Since the pressure at the nozzle exit is always higher than the ambient one, the flow pushes its way in the ambient atmosphere and forms the jet and jet shear layers. The spreading of the jet shear layer is caused by the mixing and momentum exchange in the shear layer and is very important for the noise generation (e.g. [11]).

3.3 Boundary Conditions

3.3.1 ***Inflow Boundary Condition*** At the inlet boundary, the dependent variables and their spatial derivatives are specified to be those of the ambient flow, while at the nozzle exit, the elevated pressure $p = p_e$ is imposed, *i.e.* the jet is under-expanded, as in the physical experiment.

No artificial forcing of the shear layer is imposed at the nozzle. At the surrounding and outflow boundaries, the Type I and Type II CE/SE non-reflecting boundary conditions as described in the next subsection are imposed respectively.

3.3.2 ***Non-Reflecting Boundary Conditions*** In the CE/SE scheme, non-reflecting boundary conditions (NRBC) are constructed so as to allow fluxes from the interior domain of a boundary CE to *smoothly* exit the domain [18]. There are various versions of the non-reflecting boundary condition, and in general they have proven to be well suited for aeroacoustic problems [12-17]. The following are the ones employed for the 3-D problem:

1. Type I: For a ghost grid node $(-j, n)$ lying outside the domain boundary and being a mirror image of an interior node (j, n), where j is the node index number and n the number of the time step, the non-reflecting boundary condition (type I) requires that

   $$(\boldsymbol{U}_x)^n_{-j} = (\boldsymbol{U}_y)^n_{-j} = (\boldsymbol{U}_z)^n_{-j} = 0,$$

   while $\boldsymbol{U}^n_{-j}$ is kept fixed at the initially given steady boundary value.

2. Type II: At the downstream boundary, where there are substantial gradients in the y, z directions, the non-reflective boundary condition (type II) requires that

   $$(\boldsymbol{U}_x)^n_{-j} = 0,$$

   while $\boldsymbol{U}^n_{-j}$, $(\boldsymbol{U}_y)^n_{-j}$ and $(\boldsymbol{U}_z)^n_{-j}$ are now defined by simple extrapolation from the interior, *i.e.*,

   $$\boldsymbol{U}^n_{-j} = \boldsymbol{U}^{n-1}_j,$$

   $$(\boldsymbol{U}_y)^n_{-j} = (\boldsymbol{U}_y)^{n-1}_j, (\boldsymbol{U}_z)^n_{-j} = (\boldsymbol{U}_z)^{n-1}_j.$$

These non-reflecting boundary conditions (NRBC) are consistent with their counterparts in lower dimensions (1-D and 2-D). They are simple to implement and effective as well.

4 Numerical Results

In this section, the numerical results for the 3-D under-expanded rectangular jet are presented and compared to experimental results [8]. At the moderate supersonic jet Mach number $M_j = 1.6$, the overall motion in the experiment [8] is in truly 3-D mode. For imperfectly expanded jets such as this one, a quasi-periodic shock-cell structure is formed in the jet plume. The streamwise-growing instability waves naturally occurring in the jet shear layer interact with this shock-cell structure and generate broadband shock-associated noise and under certain conditions screech tones develop through a feedback loop.

It is important to realize that even if no harmonic forcing is intentionally imposed on or introduced in the numerical simulation, the jet shear layer is in actuality continuously stimulated at a very low level as a result of truncation, round-off, and discretization errors (all of which can be characterized as numerical noise—and, in a sense, are analogous to environmental background noise in experiments). These growing perturbations interact with the shock-cell structure of the jet plume and thereby generate acoustic waves.

4.1 Test Run of Parallel Computation

Before commencing parallel computation of the rectangular jet problem, the numerical procedure is first tested on a simple jet problem with fewer grid nodes, so that it can also be run serially on a single CPU with reasonable turn-around time.

Figure 4 depicts a sketch of the simplified jet problem. The computational domain is a rectangular hexahedron. At the inlet plane, boundary conditions are set to the values of the stationary ambient flow except at the center square jet nozzle, a jet flow $M_j = 1.2$ is imposed. The stationary ambient flow is also used as the initial conditions. Type I and II NRBC's are applied accordingly. A modest grid of $30 \times 30 \times 30$ rectangular hexhedron blocks is used to generate the unstructured grid. The problem is then run first in parallel mode on an SGI workstation cluster using 8 processors of 195 MHz, and second, serially on a PC with Pentium III 600MHz CPU for 20,000 time steps. In both cases, only single precision arithmetic is used. Figure 5 illustrates the schematic diagram of the parallel computation. The computed results are practically identical, as demonstrated in Figure 6. While the computation on the serial machine takes about 9 seconds CPU time per time step, it only takes about 1 second (CPU time) per time step in the parallel mode on the SGI workstation cluster. The advantage of parallel computation is thus clearly demonstrated.

4.2 The Rectangular Jet Problem

The grid, initial and boundary conditions for the current rectangular jet problem are already described in the previous section. The actual computation was run for 60,000 time steps in order to ensure that all transients are convected out of the computational domain.

In the preprocessing stage, domain decomposition with METIS and the data setup for each processor only takes a few minutes to complete. Sixteen processors on an SGI workstation cluster are employed for the computation. These CPU's are R10000 chips ranging from 195MHz to 250 MHz in speed. With these 16 processors, the average CPU time consumption is about 5.1 second per time step. However, depending on the load of the SGI cluster, it takes about 5-6 days turn-around time to run 60,000 time steps, which is still acceptable in our view.

In the following, snapshots of flow variables are plotted and compared to available experimental results or observations. It should be emphasized that no buffer zone at the domain boundaries is used in these computations. The CE/SE NRBC is robust enough to yield a solution free of noticeable spurious reflections.

4.3 Jet Shock-Cell Structure

Experimental results for supersonic jets are often documented in terms of Schlieren pictures. It is straightforward to construct Schlieren graphs from the numerical results without loss of accuracy in view of the nature of the CE/SE method, since density derivatives are directly solved for as unknowns. Figure 7 shows a comparison of numerical Schlieren (density gradient modulus) contours from the current computations and the experimental Schlieren photograph in [8]. The numerical result is a snapshot of the instantaneous density gradient contour plot on the mid sectional plane of the narrow side at the end of the computation (60,000 time steps). The shock cells that have developed so far in the simulation agree quite well with the experimental ones. In the same Figure 7, numerical Schlieren on the mid sectional plane of the wide side is also shown. Shock-cell structures in the jet plume are clearly demonstrated.

Similar shock-cell structures are also observed from the pressure, u- velocity. and Mach number contours in Figures 8, 10, and 11.

4.4 Near-Field Jet Flow

In the computation, no artificial forcing is imposed at the nozzle exit at all, yet the shock-cell structure and instability waves seem to be sustainable (at least to the stage of 60,000 time steps). This implies a feedback loop is likely formed around the shear layer between the nozzle lip wall and the shock-cell structure, although more refined grid and much more time steps are required to verify this. (Based on our experiences with 2-D underexpanded axisymmetric sonic jet computation, screech wave takes place when the grid is fine enough.)

Figure 8 shows the isobars on the mid sectional planes of both the narrow and the wide sides. Similar shock-cell structures as in Figure 7 are found. Pressure isosurfaces at two close but different levels are plotted in Figure 9. It is clearly demonstrated that these pressure waves at the two edges of the wide side jet plume form a helical pattern. Qualitatively, this pattern agrees with the observation of Quinn [20] and with the observation of Westley and Woolley [19] on screech of spinning mode. Although these waves look like Mach radiation, at the present stage, with a very coarse grid of about 1.7 million cells, it is not sure if these pressure waves are truly radiating Mach waves. Investigation with a finer grid is needed.

Figure 10 illustrates the u velocity contours at the mid-sectional planes of the narrow and wide sides. The outskirts of the jet plume on the narrow side form barrel-like shapes according to the shock-cell structure and spread out due to mixing. This is in contrast to the axisymmetric mode, where the outskirts of the jet plume form only smooth lines. Another interesting observation from the numerical results is the "axis switching" phenomenon, the jet core seems to keep reducing its width on the wide side and increasing its width on the narrow side due to shear layer spreading. Therefore, a few diameters (D) downstream from the nozzle exit, the jet core appears to be roundish, although at the nozzle exit it is rectangular with an aspect ratio of about 5. The same observation can also be found in Figure 11.

5 Concluding Remarks

In this paper, the recent unstructured CE/SE Euler scheme is extended to 3-D computation for a supersonic under-expanded rectangular jet. The state-of-the-art techniques of METIS and MPI are applied in the parallelization of the unstructured CE/SE Euler code, and proved to be effective and efficient.

The advantages of the CE/SE scheme found previously in 2-D computations are confirmed again for 3-D simulations:

1. The method is robust and the implementation is 'effortless' in that no special treatment and parameter selections are needed;

2. The NRBC is simple and effective, no buffer zone is used;

3. The method handles both linear and nonlinear problems and is particularly advantageous for near field jet-noise computation;

4. Unstructured grid and parallelization help to handle large scale problems with complicated geometry.

With a very modest unstructured grid of about 1.7 million elements (cells) and single precision computation, many aspects of the computed results are in good qualitative agreement with experimental findings [8], [20]. With 16 processors in an SGI workstaion cluster, the CPU time consumed per time step is about 4 seconds. However, a self-sustained oscillation, *i.e.* the screech tone, is yet to be achieved in our simulation. At the nozzle lip, a finite lip wall is already added to facilitate the forming of the feedback loop. Based on current encouraging results of 2-D axisymmetric jet screech tone computation, we are sure the screech can be computed with refined grid. Also, in order to achieve a more physically relevant simulation, a Navier-Stokes CE/SE code with LES (large eddy simulation) or turbulence modeling capability is need to account for the strong momentum exchange in the shear layer. The results will be reported in the future.

6 Acknowledgements

The authors wish to thank Dr. L.S. Hultgren for fruitful discussions. This work received support from the Supersonic Propulsion Technology Project Office of NASA Glenn Research Center.

References

[1] Wang,X.Y. and Chang, S. C., "A 3-D Non-splitting Structured/unstructured Euler Solver Based on the Space-Time Conservation Element and Solution Element Method', AIAA Paper, 99-3278, in "A Collection of the 14th AIAA Computational Fluid Dynamics Conference Technical Papers", Norfolk, VA, June-July, 1999.

[2] Himansu, A., Jorgenson, P.C.E., Wang, X.Y., and Chang, S. C., " Parallel CE/SE Computations via Domain Decomposition", to be presented at the First International Conference on Computational Fluid Dynamics" (ICCFD), Kyoto, Japan, July,2000.

[3] Karypis, G. and Kumar, V., " Multilevel k-way Partitioning Scheme for Irregular Graphs", Univ. of Minnesota Dept. of Comp. Sc. / Army HPC Research Center Tech. Report 95-064

[4] refer to website: http://www-unix.mcs.anl.gov/mpi

[5] Chang, S. C., "The Method of Space-Time Conservation Element and Solution Element—A New Approach for Solving the Navier-Stokes and Euler Equations," J. Comput. Phys. v. 119, 295-324 (1995).

[6] Chang, S. C., Yu, S. T., Himansu, A., Wang, X. Y., Chow, C. Y. and Loh, C. Y., "The Method of Space-Time Conservation Element and Solution Element—A New Paradigm for Numerical Solution of Conservation Laws", *Computational Fluid Dynamics Review*, eds. M. M. Hafez and K. Oshima, Wiley (1997).

[7] Chang, S.-C., Wang, X.-Y. and Chow, C.-Y., "The Space-Time Conservation Element and Solution Element Method—A New High Resolution and Genuinely Multidimensional Paradigm for Solving Conservation Laws", *J. Comp. Phys.*, **156** (1999), pp. 89-136.

[8] Raman, G., " Cessation of Screech in underexpanded jets", *J. Fluid Mech.*, v. 336, pp. 69-90 (1997).

[9] Raman G., "Advancces in Understanding Supersonic Jet Screech: Review and Perspective," Prog. Aerospace Sci. v. 34, pp. 45-106 (1998).

[10] Tam, C. K .W., "Supersonic Jet Noise," Ann. Rev. Fluid Mech. v. 27, pp. 17-43 (1995).

[11] Tam, C. K. W., "Jet Noise Generated by Large Scale Coherent Motion," NASA RP-1258, pp 311-390 (1991).

[12] Loh, Ching Y., Hultgren, Lennart S. and Sin-Chung Chang, "Computing Waves in Compressible Flow Using the Space-Time Conservation Element Solution Element Method," AIAA Paper 98-0369 (1998).

[13] Loh, C. Y., Hultgren, L. S., Chang, S.-C. and Jorgenson, P. C. E., "Vortex Dynamics Simulation in Aeroacoustics by the Space-Time Conservation Element Solution Element Method," AIAA Paper 99-0359 (1999).

[14] Loh, C. Y., Chang, S. C., Scott, J. R., and Yu, S. T., "Application of the Method of Space-Time Conservation Element and Solution Element to Aeroacoustics Problems," presented at 6th International Symposium of CFD, Lake Tahoe, California (1995).

[15] Loh, C. Y., Chang, S. C., Scott, J. R., and Yu, S. T., "The Space-Time Conservation Element Method—A New Numerical Scheme for Computational Aeroacoustics ", AIAA Paper 96-0276 (1996).

[16] Loh, C. Y., Chang, S. C. and Scott, J. R., "Computational Aeroacoustics via the Space-Time Conservation Element/Solution Element Method", AIAA Paper 96-1687 (1996).

[17] Chang, S. C., Loh, C. Y. and Yu, S. T., "Computational Aeroacoustics via a New Global Conservation Scheme", *Proceedings of the 15th International Conference on Numerical Methods in Fluid Dynamics*, eds. P. Kutler, J. Flores and J.-J. Chattot, June 24-28, 1996, Monterey, CA (1997).

[18] Chang, S. C., Himansu, A., Loh, C. Y., Wang, X. Y., Yu, S.-T. and Jorgenson, P. C. E. "Robust and Simple Non-Reflecting Boundary Conditions for the Space-Time Conservation Element and Solution Element Method", AIAA Paper 97-2077 (1997).

[19] Westley, R. and Woolley, J.H., " An Investigation of the near noise field of a choked axisymmetric jet", National Research Council of Canada, NAE, Aeronautical Reprot LR-506, (1968).

[20] Quinn, W.R., " Development of a Large Aspect-Ratio Rectangular Turbulent Free Jet", AIAA J. Vol. 32, No.3, pp. 547-554 (1994).

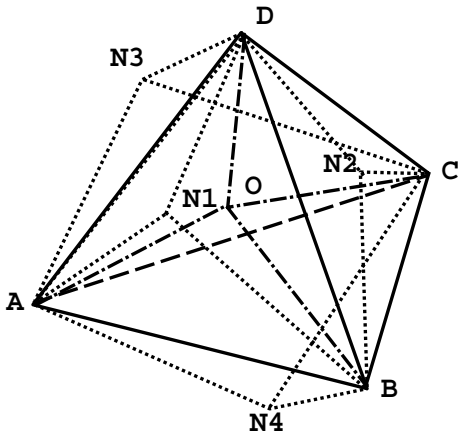

A,B,C,D - tetrahedron vertices, O - cell center, N1,N2,N3,N4 - neighboring cell centers

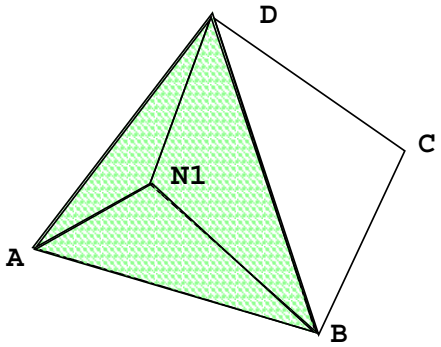

showing part of the hexahedron O-ABD-N1 (shaded area)

Figure 1: Tetrahedron and dodecahedron in an unstructured grid.

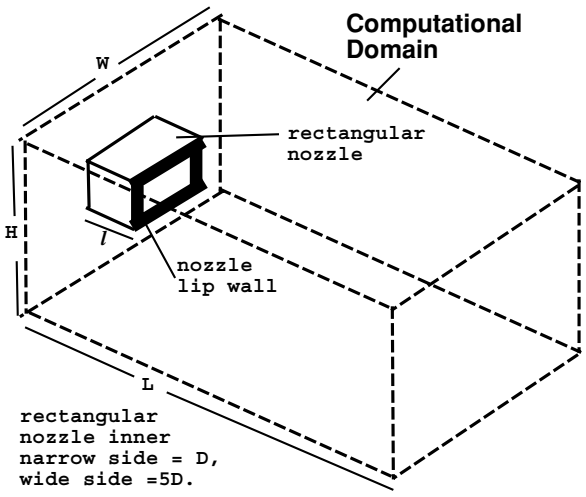

Figure 2: Sketch of the rectangular jet problem.

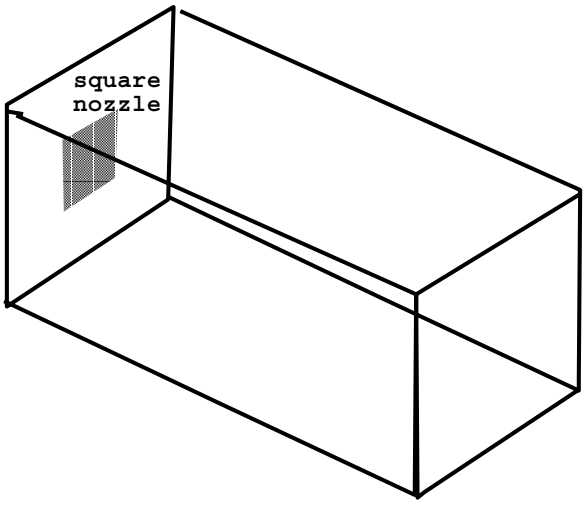

Figure 4: Sketch of the test problem.

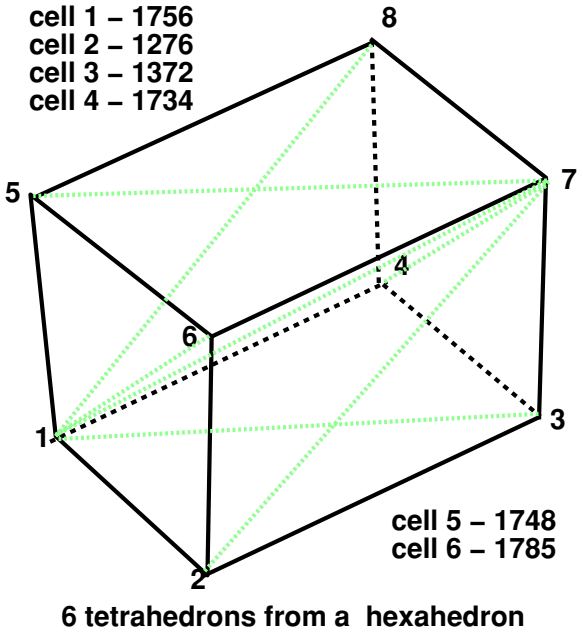

Figure 3: Partition of a hexahedron into 6 tetrahedrons.

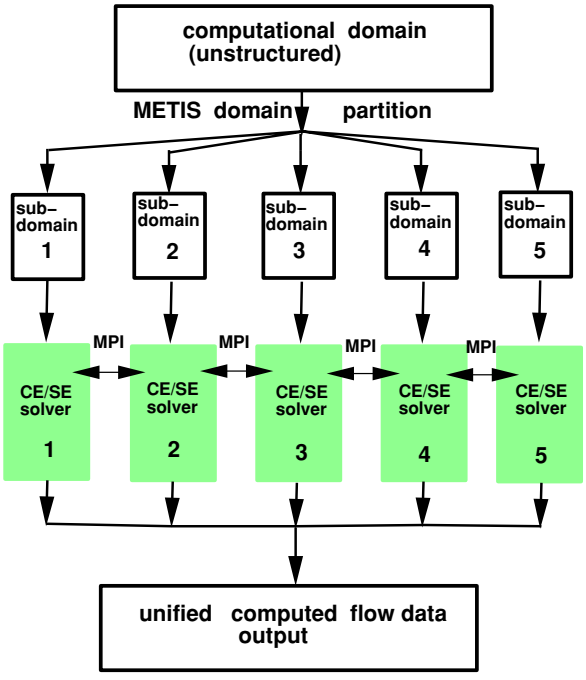

Figure 5: Schematic diagram of parallel computation (showing 5 processors).

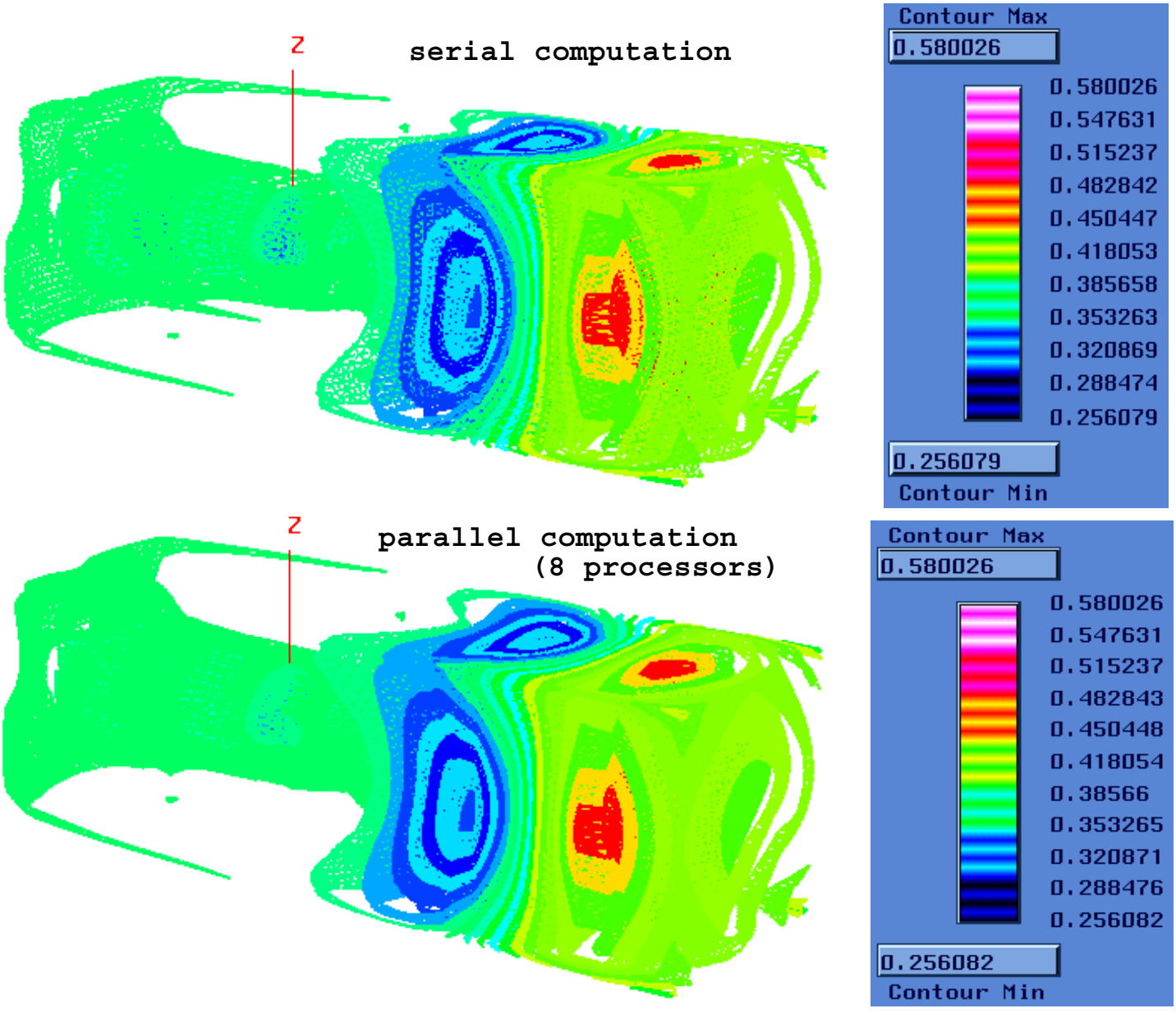

Figure 6: Comparison of numerical results by parallel and serial computations.

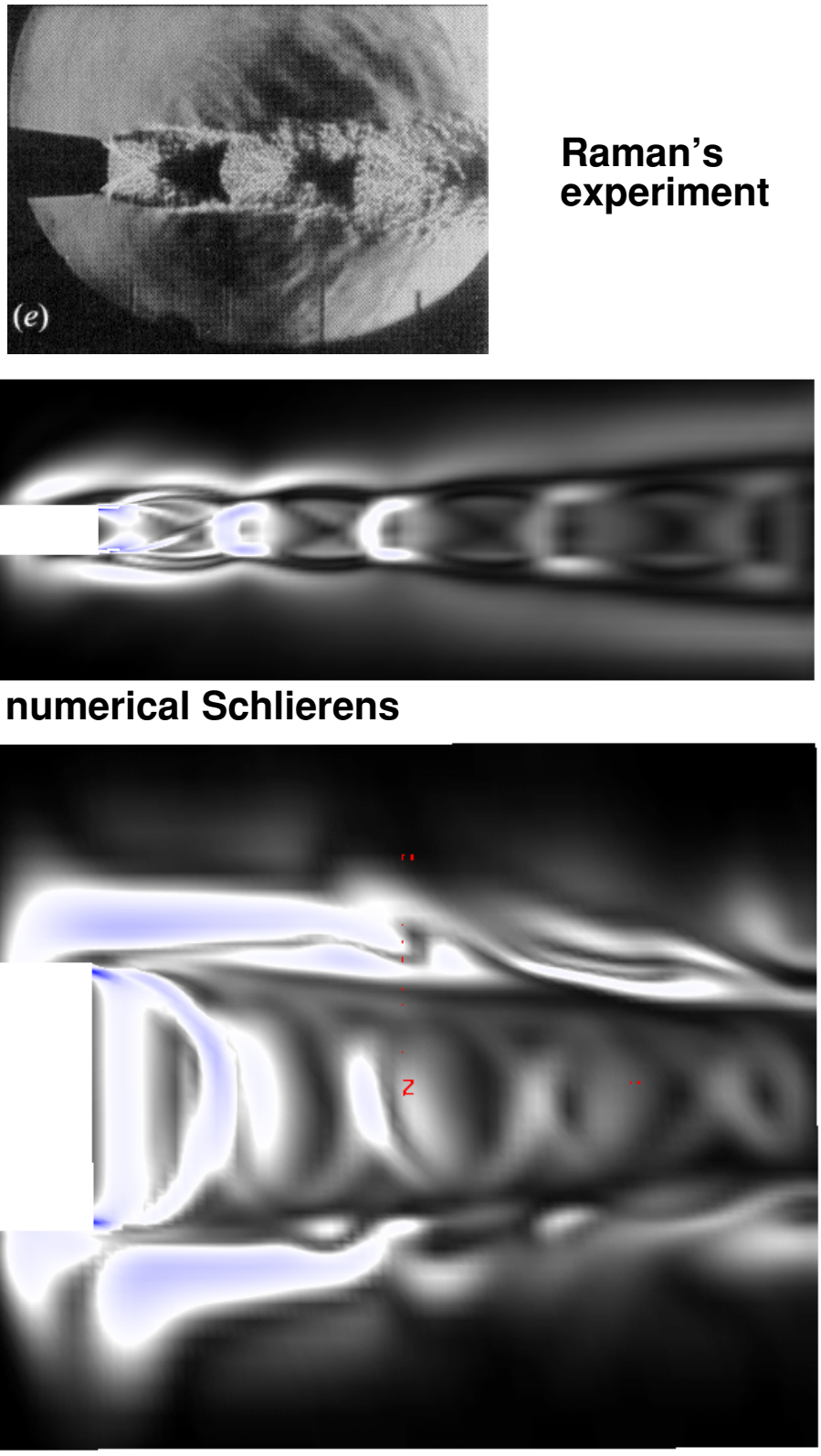

Figure 7: Comparison of numerical Schlieren graph (instantaneous snapshot) and the experimental time averaged Schlieren graph ; showing good agreement of the first few shock cells.

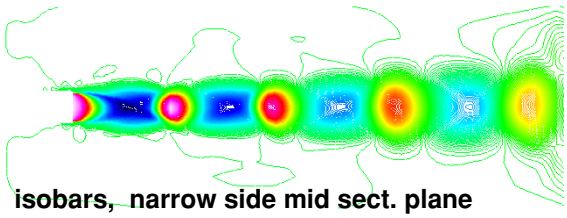

isobars, narrow side mid sect. plane

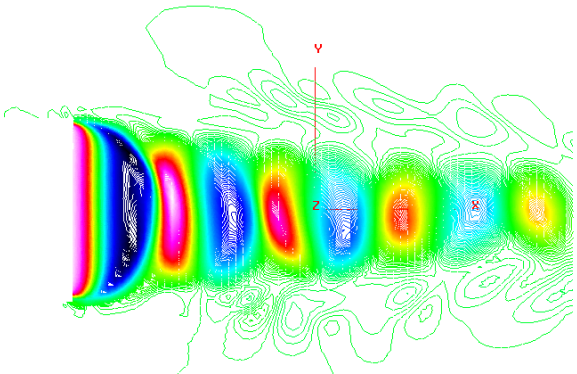

isobars, wide side mid sect. plane

Figure 8: Pressure contours on the narrow and wide side mid sectional planes.

u–contours, narrow side mid sectional plane

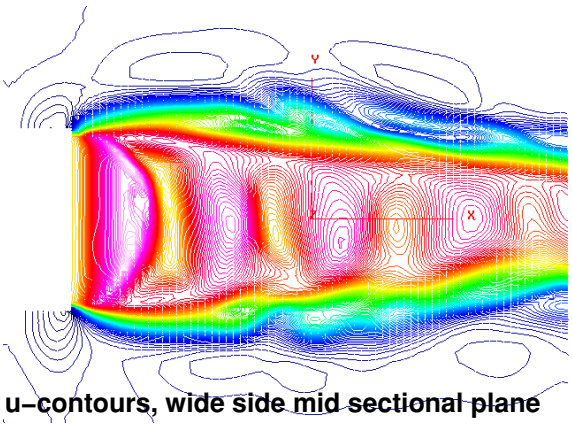

u–contours, wide side mid sectional plane

Figure 10: u- velocity contours

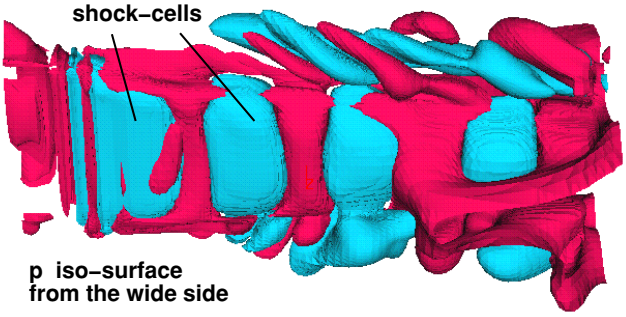

p iso–surface
from the wide side

low level: p=.274, high level: p=.2792

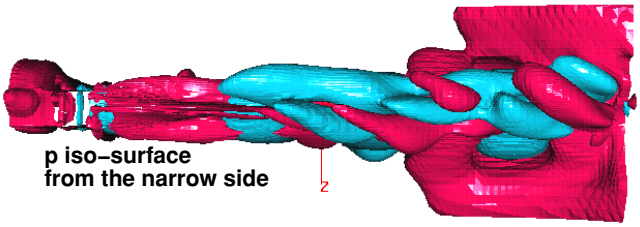

p iso–surface
from the narrow side

Figure 9: Pressure iso-surfaces at 2 different levels, showing the shock-cells, the helical Mach radiations.

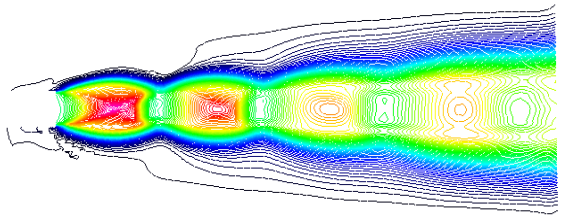

M, narrow side mid sectional plane

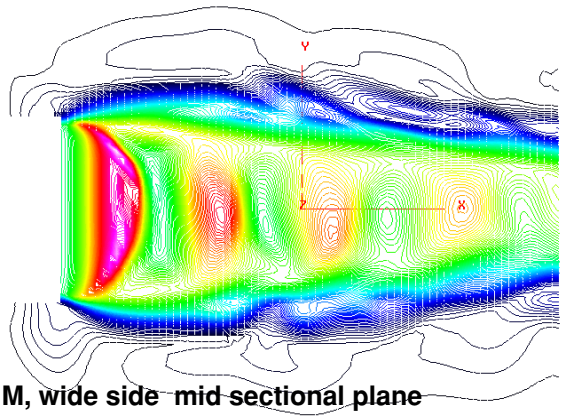

M, wide side mid sectional plane

Figure 11: Mach number contours.

REPORT DOCUMENTATION PAGE

Form Approved
OMB No. 0704-0188

1. AGENCY USE ONLY (*Leave blank*)	2. REPORT DATE	3. REPORT TYPE AND DATES COVERED
	December 2000	Technical Memorandum

4. TITLE AND SUBTITLE

Computation of an Underexpanded 3-D Rectangular Jet by the CE/SE Method

5. FUNDING NUMBERS

WU–708–90–43–00

6. AUTHOR(S)

Ching Y. Loh, Ananda Himansu, Xiao Y. Wang, and Philip C.E. Jorgenson

7. PERFORMING ORGANIZATION NAME(S) AND ADDRESS(ES)

National Aeronautics and Space Administration
John H. Glenn Research Center at Lewis Field
Cleveland, Ohio 44135–3191

8. PERFORMING ORGANIZATION REPORT NUMBER

E–12552

9. SPONSORING/MONITORING AGENCY NAME(S) AND ADDRESS(ES)

National Aeronautics and Space Administration
Washington, DC 20546–0001

10. SPONSORING/MONITORING AGENCY REPORT NUMBER

NASA TM—2000-210594
AIAA–2001–0986

11. SUPPLEMENTARY NOTES

Prepared for the 39th Aerospace Sciences Meeting and Exhibit sponsored by the American Institute of Aeronautics and Astronautics, Reno, Nevada, January 8–11, 2001. Ching Y. Loh, Ananda Himansu, and Xiao Y. Wang, Taitech Inc., Cleveland, Ohio 44135 (work funded by NASA Contract NAS3–97186); and Philip C.E. Jorgenson, NASA Glenn Research Center. Responsible person, Philip C.E. Jorgenson, organization code 5880, 216–433–5386.

12a. DISTRIBUTION/AVAILABILITY STATEMENT

Unclassified - Unlimited
Subject Categories: 01, 45, and 64 Distribution: Nonstandard

Available electronically at http://gltrs.grc.nasa.gov/GLTRS

This publication is available from the NASA Center for AeroSpace Information, 301–621–0390.

12b. DISTRIBUTION CODE

13. ABSTRACT ***(Maximum 200 words)***

Recently, an unstructured three-dimensional space-time conservation element and solution element (CE/SE) Euler solver was developed. Now it is also developed for parallel computation using METIS for domain decomposition and MPI (message passing interface). The method is employed here to numerically study the near-field of a typical 3-D rectangular under-expanded jet. For the computed case—a jet with Mach number $M_j = 1.6$, with a very modest grid of 1.7 million tetrahedrons, the flow features such as the shock-cell structures and the axis switching, are in good qualitative agreement with experimental results.

14. SUBJECT TERMS

Computational aeroacoustics; CE/SE method

15. NUMBER OF PAGES

17

16. PRICE CODE

A03

17. SECURITY CLASSIFICATION OF REPORT	18. SECURITY CLASSIFICATION OF THIS PAGE	19. SECURITY CLASSIFICATION OF ABSTRACT	20. LIMITATION OF ABSTRACT
Unclassified	Unclassified	Unclassified	